**Electronic Supplementary Information for**

# Conjugated coordination polymer enables efficient proton supply on platinum surface for alkaline hydrogen evolution electrocatalysis

Shuting Zhan[a], Yunxia Liu[b], Xinyue Xu[a], Yan Liu[c], Ziwei Ma[a], Shouhan Zhang[a], Li Hu[a], Haiping Lin[d], Longsheng Zhang*[a] and Tianxi Liu[a]

[a]*Key Laboratory of Synthetic and Biological Colloids, Ministry of Education, School of Chemical and Material Engineering, Jiangnan University, Wuxi 214122, China*

[b]*School of Chemistry and Chemical Engineering, Northwestern Polytechnical University, Xi'an 710072, China*

[c]*Department of Chemistry, National University of Singapore, Singapore 117543, Singapore*

[d]*School of Physics and Information Technology, Shaanxi Normal University, Xi'an 710062, China*

[*]*Corresponding author. E-mail: zhangls@jiangnan.edu.cn*

## Experimental Section

### Characterization

XRD patterns of samples were collected from a MiniFlex600 X-ray diffractometer with Cu $K_\alpha$ radiation ($\lambda$ = 0.1542 nm). Morphologies of samples were observed through using TEM (JEM-2100F, JEOL and Talos F200X G2, FEI). The weight percentage of Pt in the samples was quantified via inductively coupled plasma-mass spectrometry (ICP-MS, iCAP Pro, Thermo Fisher). XPS spectra of samples were obtained from a Shimadzu/Krayos AXIS Ultra DLD device.

### Electrochemical active surface area (ECSA) calculation

The ECSA of catalysts were calculated based on their electrical double layer capacitor ($C_{dl}$), which were obtained from cyclic voltammetry (CV) plots in a narrow non-Faradaic potential window from −0.80 to −0.90 V (vs. Hg/HgO). The anodic currents at 0 V (vs. Hg/HgO) were plotted as a function of scan rate. Then linear fitting was adopted to these points, and the slope of plots gives the value of $C_{dl}$. The specific capacitance was found to be 30 μF $cm^{-2}$, and the ECSA values were calculated from Equation 1:

$$ECSA = \frac{Cdl}{30\ \mu F/cm^2}\, cm^2 \tag{1}$$

### Turnover frequency (TOF) calculation

The TOF values of catalysts were calculated from Equation 2:

$$TOF = \frac{j \times A}{2 \times F \times n} \tag{2}$$

where *j* is the current density obtained at −0.1 V (vs. reversible hydrogen electrode, RHE), A is −the geometric area, F is the Faraday constant and n is the mole number of Pt atoms, which was calculated *via* Equation 3:

$$n = \frac{m_{loading}}{Mw} \tag{3}$$

where $m_{loading}$ is the loading mass of Pt atoms on electrode, M is the atomic mass. The loading mass of Pt atoms in samples were based on the ICP-MS analysis.

**Alkaline water electrolyzer**

The FAA-3-PK-130 anionic membrane purchased from Suzhou Shengernuo was used as the polymer electrolyte membrane. Iridium oxide ($IrO_2$, damas beta, 99.9%) was used as the anode catalyst, while the cathode catalyst was Pt/Ni-CCP. As a benchmark, Pt/C catalyst consisted of 20% Pt obtained from Sigma-Aldrich was employed for the cathode catalyst comparison. Typically, for the anode, 10 mg $IrO_2$ and 100 μL Nafion solution were dispersed in 400 μL isopropanol while 2.5 mg Pt/C and 80 μL Nafion solution were mixed in 500 μL ethanol for the cathode to create the homogenous ink. The catalyst ink was then subjected to ultrasonic homogenization for 60 mins and later dropped on the carbon paper carefully. The final loading of catalyst layers was 0.47 mg $cm^{-2}$ for Pt/C at the cathode and 1.2 mg $cm^{-2}$ for $IrO_2$ at the anode, respectively. The full cell features a material of titanium as the current collector. Both sides of the cell incorporate serpentine flow channels, each covering an area of 1 $cm^2$. The cells were compressed using a torque of 4 N·m on each of the four bolts. The 1 M KOH aqueous solution at room temperature (25 ˚C) was continuously pumped into the anode side of the cell at a flow rate of 20 mL/min. Following the conditioning process, a polarization test was conducted using LSV at 10 mV $s^{-1}$. The current density was set at specific value of 100 mA $cm^{-2}$ for the durability test.

## Supplementary Figures

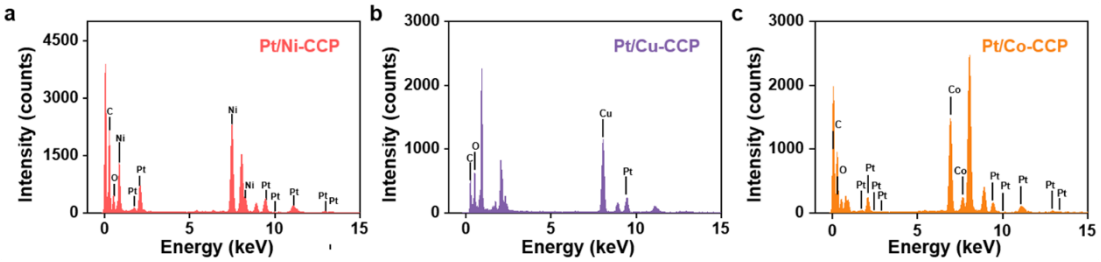


**Fig. S1.** (a–c) Energy dispersive spectroscopy results for Pt/Ni-CCP, Pt/Cu-CCP and Pt/Co-CCP, respectively.

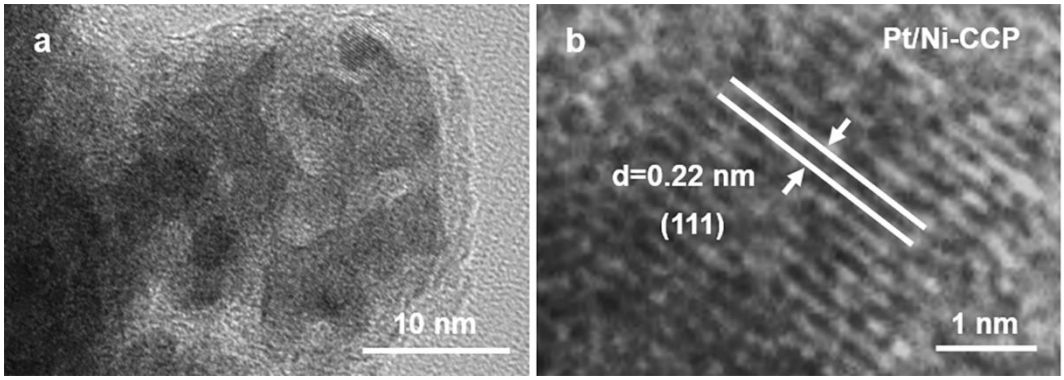


**Fig. S2.** (a, b) TEM images of Pt/Ni-CCP.

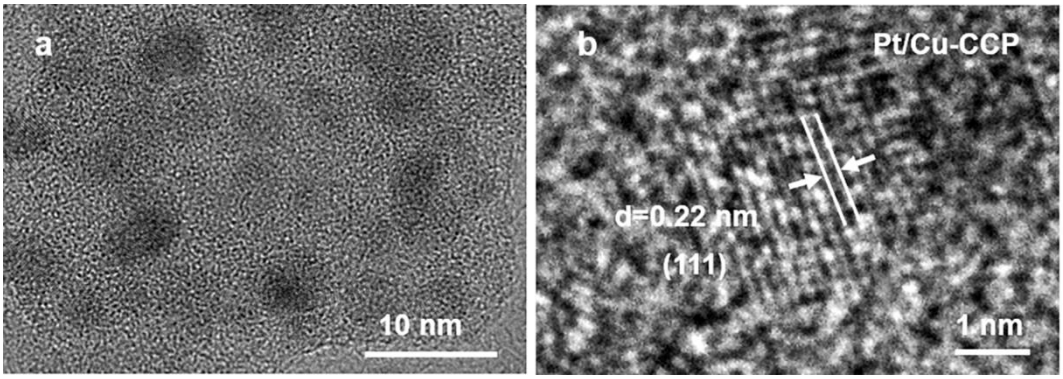


**Fig. S3.** (a, b) TEM images of Pt/Cu-CCP.

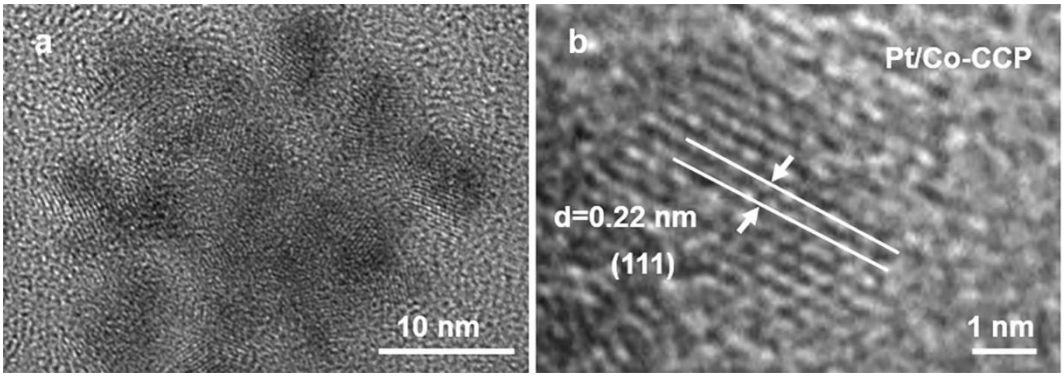


**Fig. S4.** (a, b) TEM images of Pt/Co-CCP.

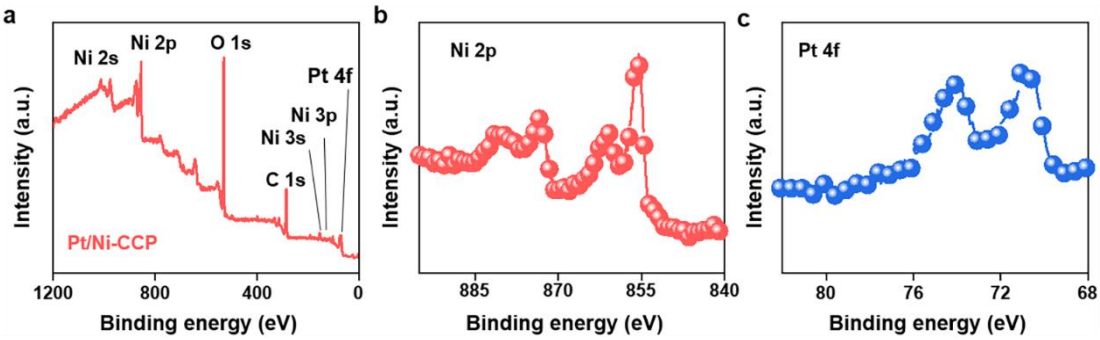


**Fig. S5.** (a–c) Full-spectrum, Ni 2p and Pt 4f XPS curves of Pt/Ni-CCP.

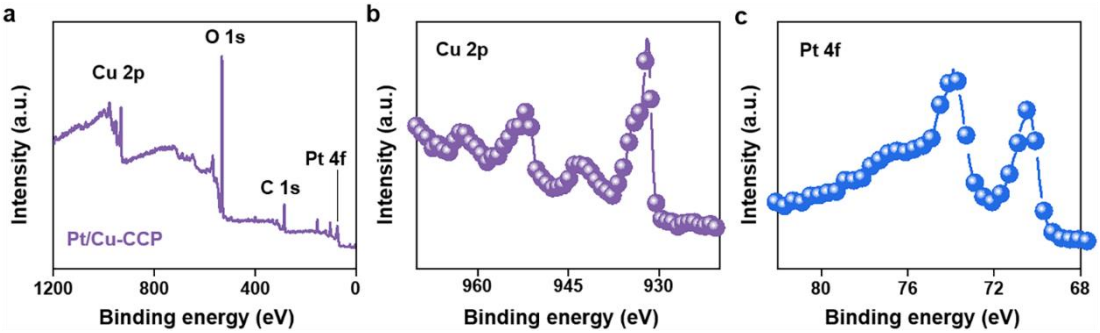


**Fig. S6.** (a–c) Full-spectrum, Cu 2p and Pt 4f XPS curves of Pt/Cu-CCP.

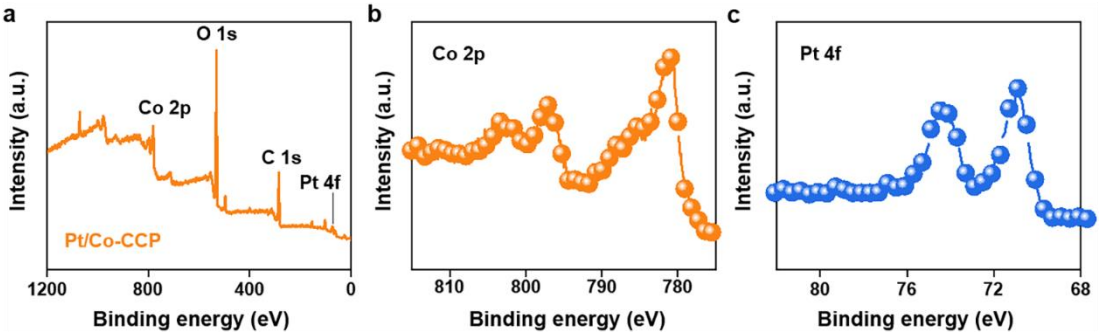


**Fig. S7.** (a–c) Full-spectrum, Co 2p and Pt 4f XPS curves of Pt/Co-CCP.

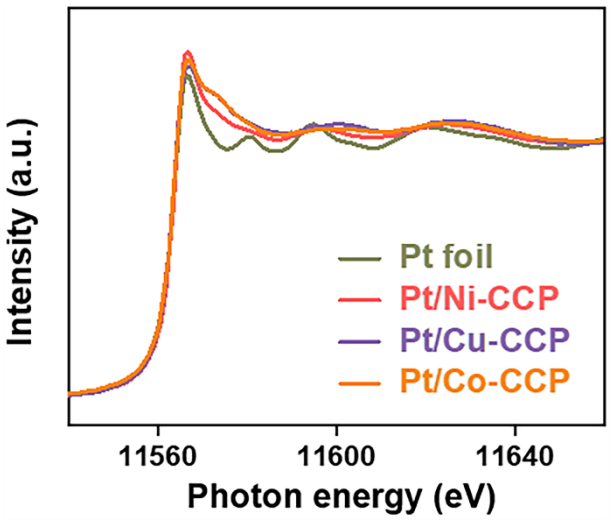


**Fig. S8.** Pt $L_3$-edge XANES spectra of Pt/Ni-CCP, Pt/Cu-CCP, Pt/Co-CCP and Pt foil.

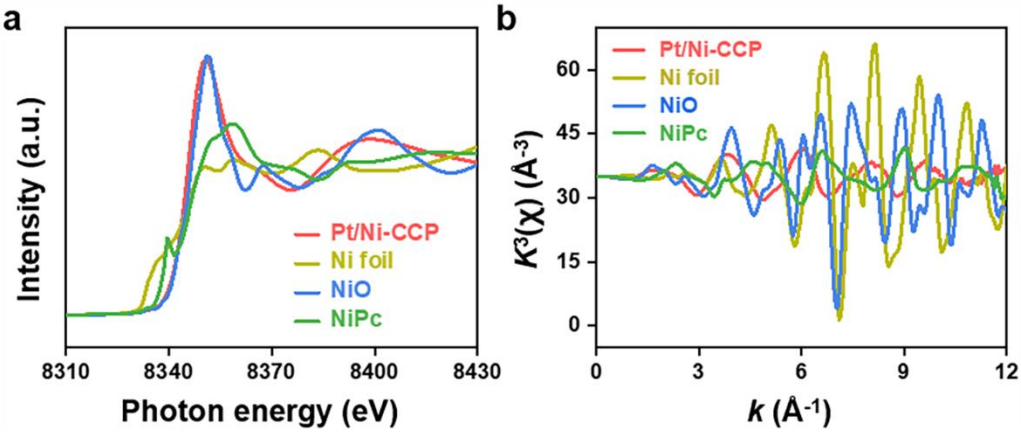


**Fig. S9.** (a) Ni *k*-edge XANES spectra for Pt/Ni-CCP, Ni foil, NiO and NiPc. (b) Ni *k*-edge EXAFS spectra for Ni foil, NiO and NiPc at *k* space.

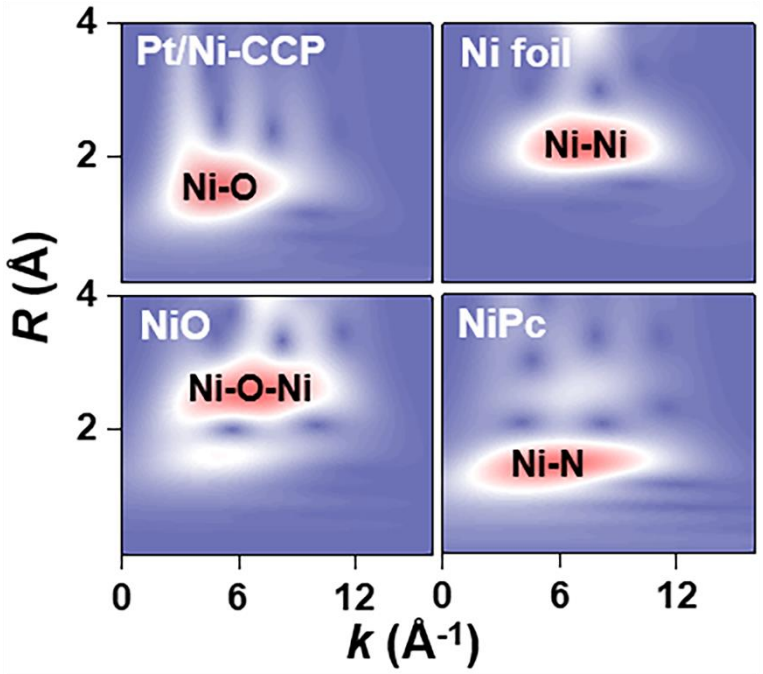


**Fig. S10.** Wavelet-transform analysis of Ni *k*-edge EXAFS spectra for Pt/Ni-CCP, Ni foil, NiO and NiPc.

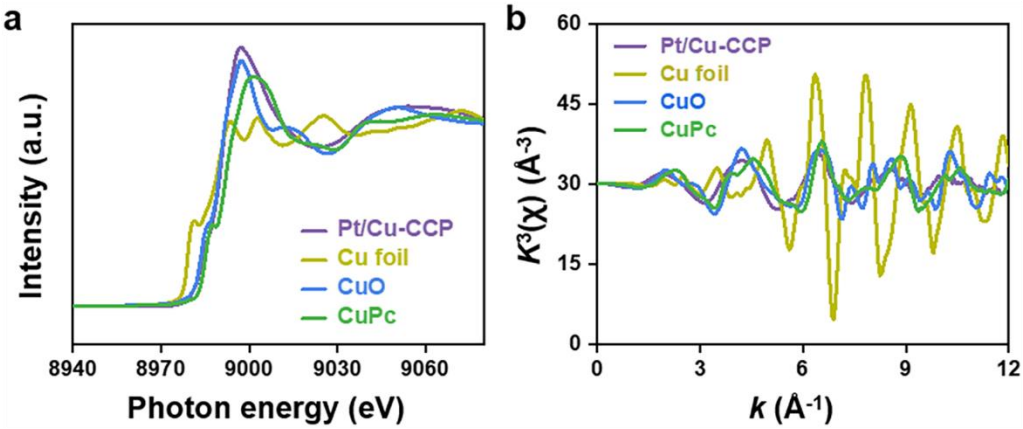


**Fig. S11.** (a) Cu *k*-edge XANES spectra for Pt/Cu-CCP, Cu foil, CuO and CuPc. (b) Cu *k*-edge EXAFS spectra for Cu foil, CuO and CuPc at *k* space.

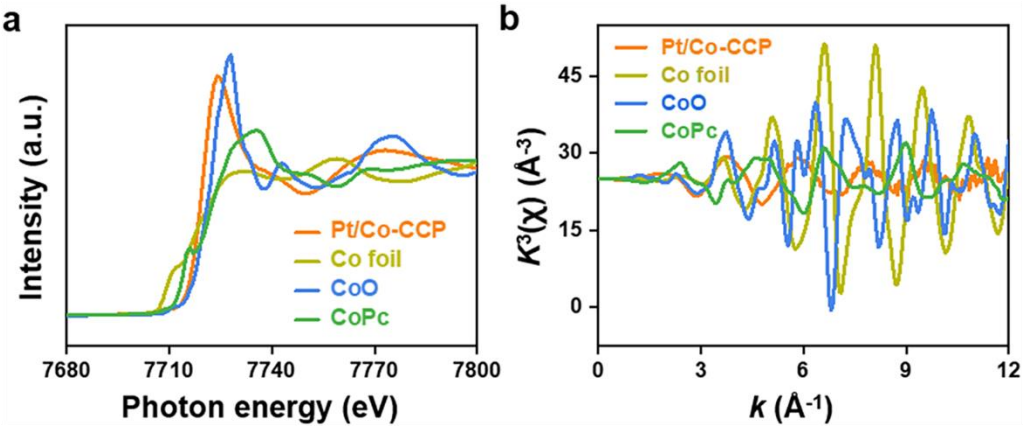


**Fig. S12.** (a) Co *k*-edge XANES spectra for Pt/Co-CCP, Co foil, CoO and CoPc. (b) Co *k*-edge EXAFS spectra for Co foil, CoO and CoPc at *k* space.

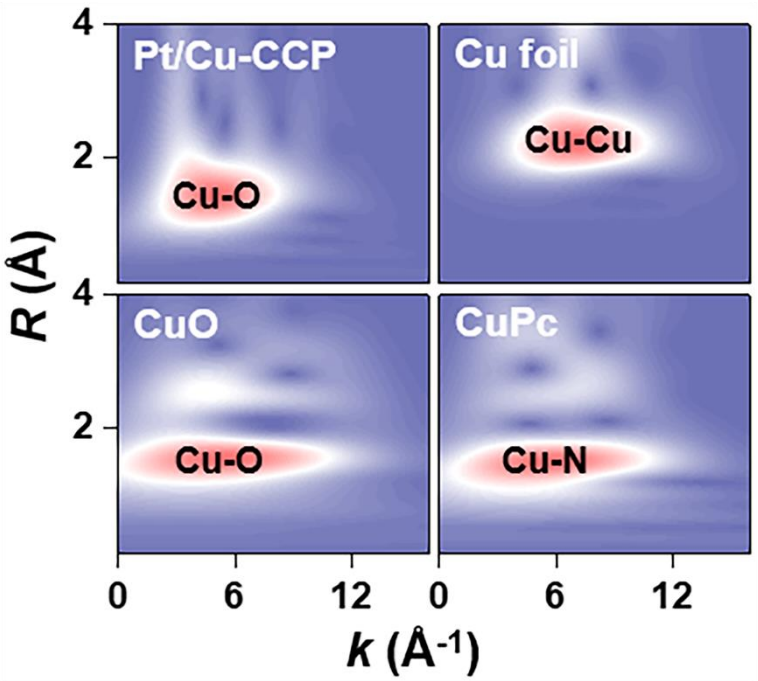


**Fig. S13.** Wavelet-transform analysis of Cu *k*-edge EXAFS spectra for Pt/Cu-CCP, Cu foil, CuO and CuPc.

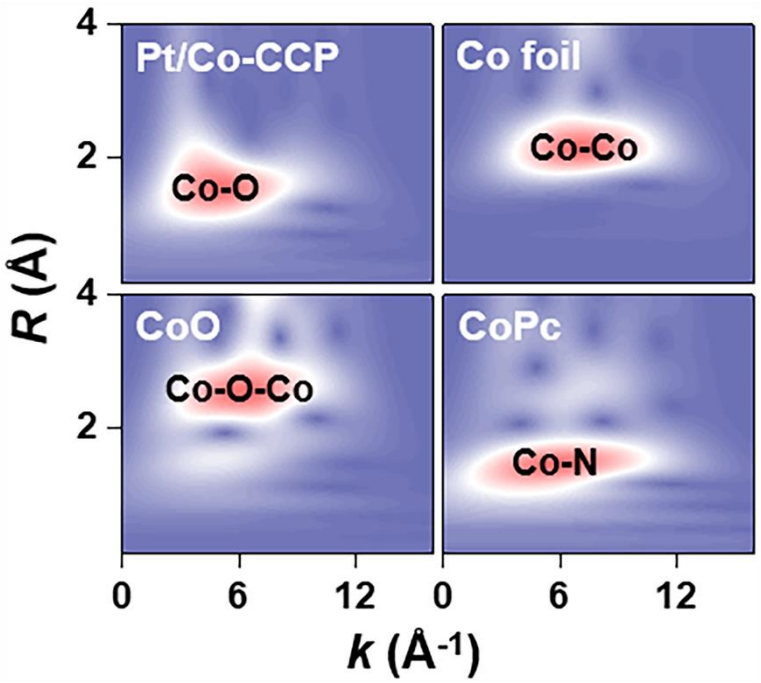


**Fig. S14.** Wavelet-transform analysis of Co *k*-edge EXAFS spectra for Pt/Co-CCP, Co foil, CoO and CoPc.

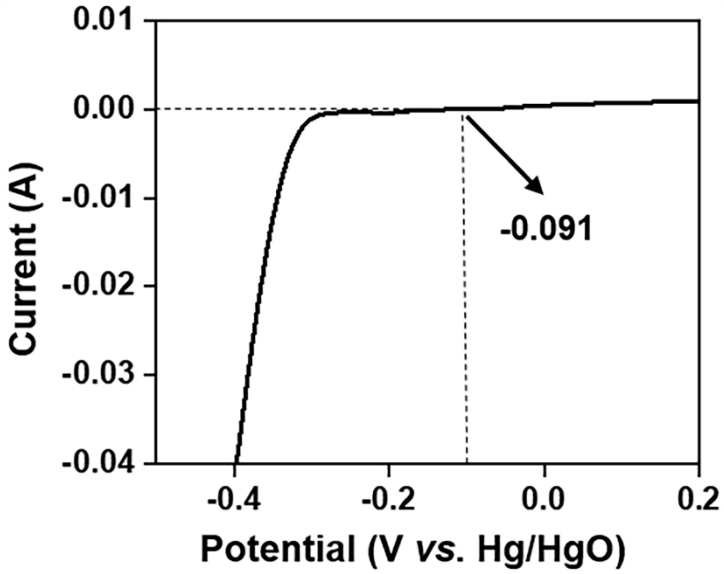


**Fig. S15.** Calibration experiment for the Hg/HgO reference electrode.

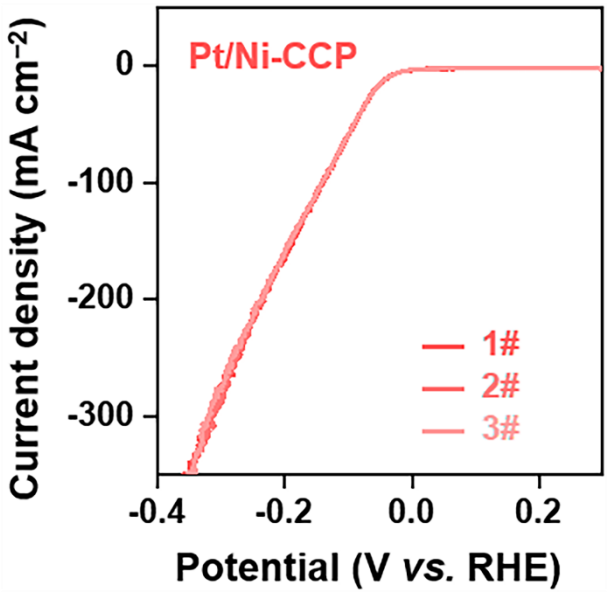


**Fig. S16.** Three independent LSV tests for the Pt/Ni-CCP catalyst measured at a scan rate of 10 mV $s^{-1}$ in 1 M KOH aqueous electrolyte.

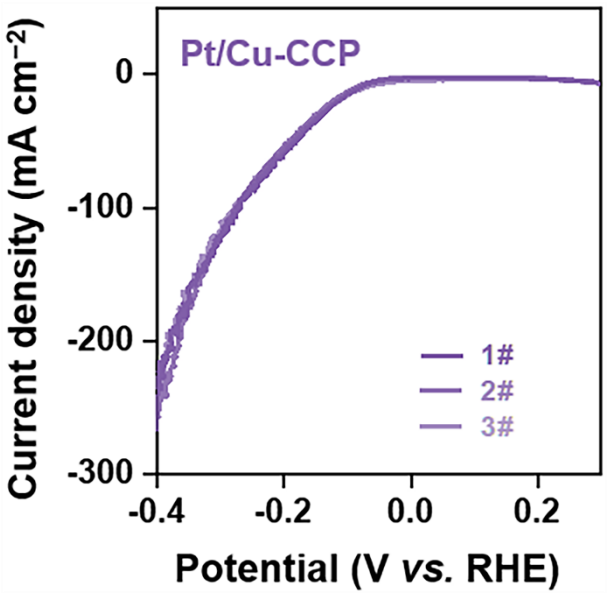


**Fig. S17.** Three independent LSV tests for Pt/Cu-CCP catalyst measured at a scan rate of 10 mV $s^{-1}$ in 1 M KOH aqueous electrolyte.

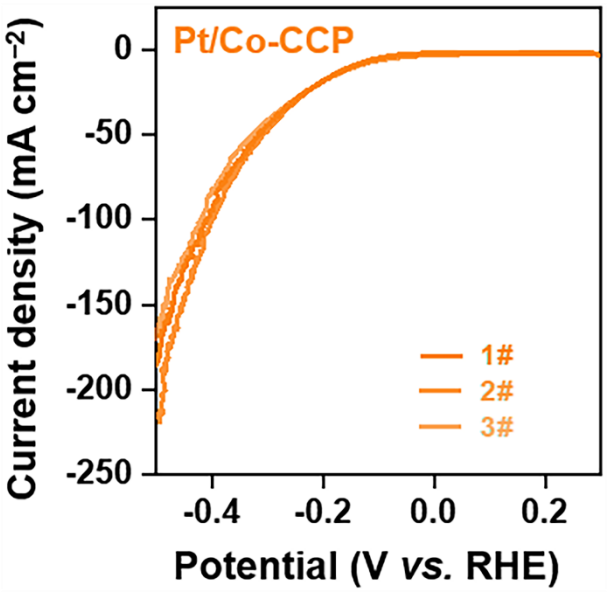


**Fig. S18.** Three independent LSV tests for the Pt/Co-CCP catalyst measured at a scan rate of 10 mV $s^{-1}$ in 1 M KOH aqueous electrolyte.

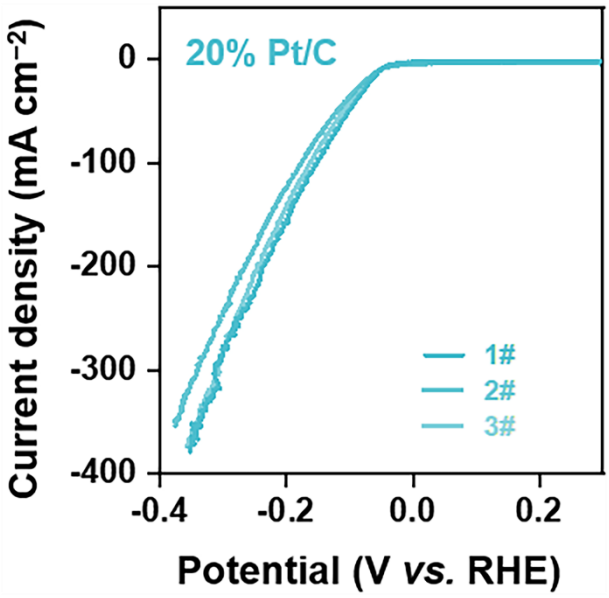


**Fig. S19.** Three independent LSV tests for the commercial Pt/C catalyst measured at a scan rate of 10 mV $s^{-1}$ in 1 M KOH aqueous electrolyte.

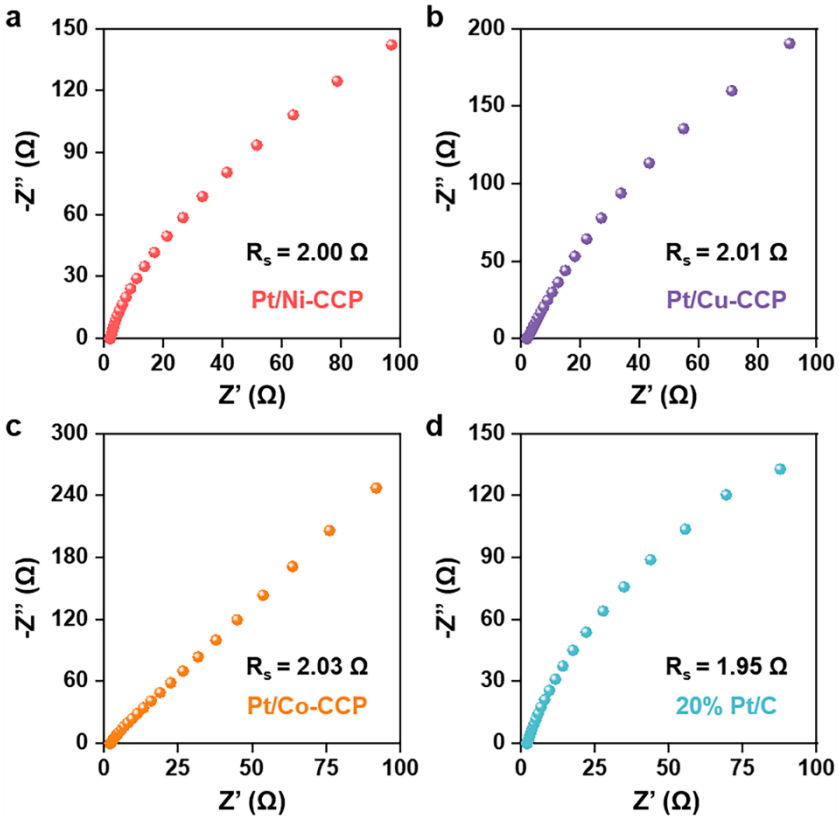


**Fig. S20.** (a−d) EIS measurements for the Pt/Ni-CCP, Pt/Cu-CCP, Pt/Co-CCP and commercial Pt/C catalysts, respectively.

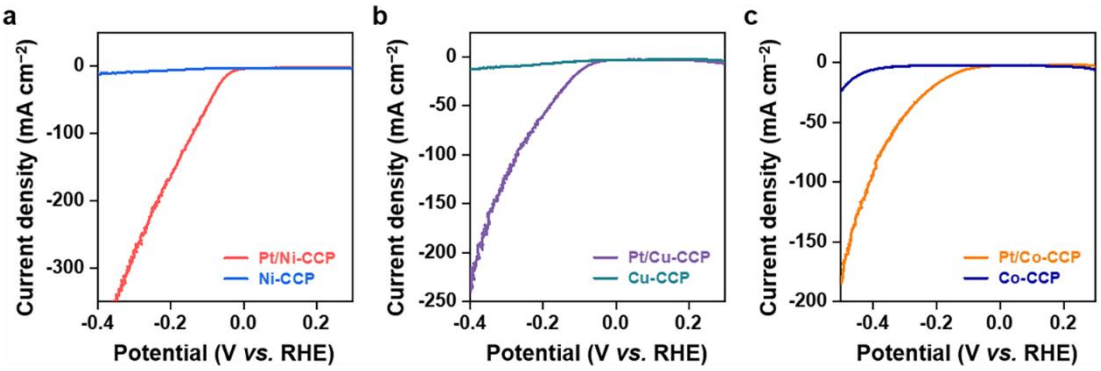


**Fig. S21.** LSV tests for (a) Pt/Ni-CCP and Ni-CCP, (b) Pt/Cu-CCP and Cu-CCP, (c) Pt/Co-CCP and Co-CCP, respectively.

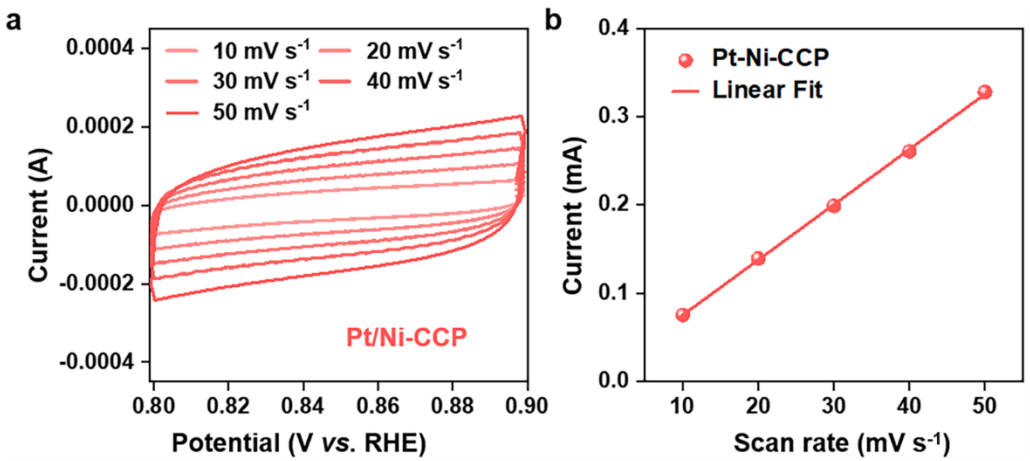


**Fig. S22.** (a) CV curves recorded at different scan rates for Pt/Ni-CCP catalyst in a non-Faradaic potential window from 0.80 V to 0.90 V (vs. RHE). (b) Current as a function of scan rate to give the $C_{dl}$ value for the Pt/Ni-CCP catalyst.

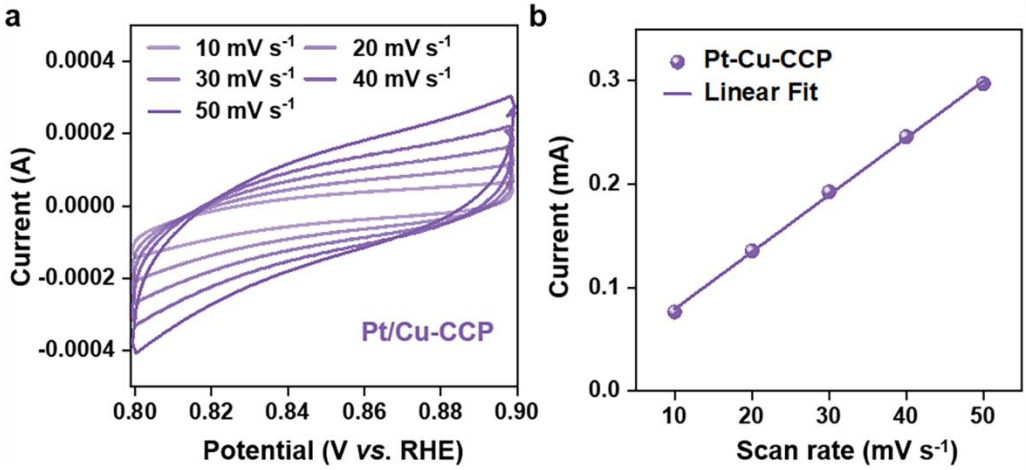


**Fig. S23.** (a) CV curves recorded at different scan rates for Pt/Cu-CCP catalyst in a non-Faradaic potential window from 0.80 V to 0.90 V (vs. RHE). (b) Current as a function of scan rate to give the $C_{dl}$ value for the Pt/Cu-CCP catalyst.

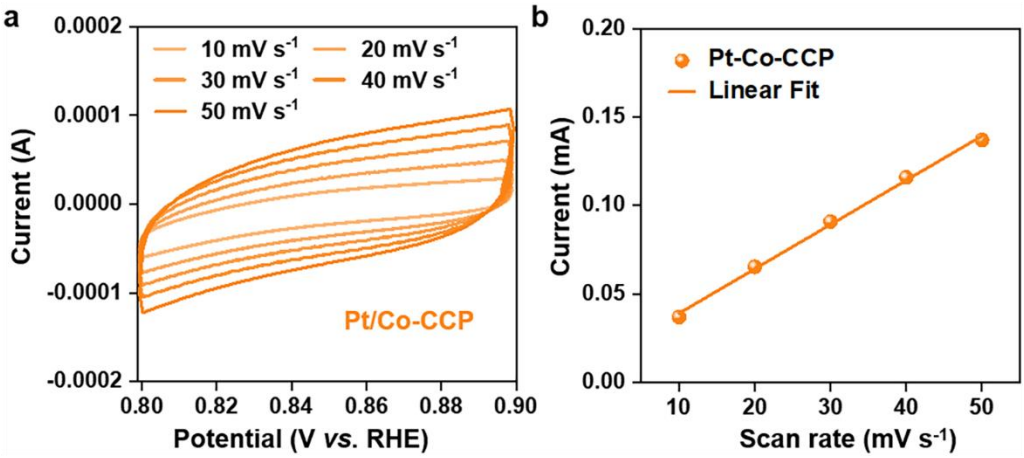


**Fig. S24.** (a) CV curves recorded at different scan rates for Pt/Co-CCP catalyst in a non-Faradaic potential window from 0.80 V to 0.90 V (vs. RHE). (b) Current as a function of scan rate to give the $C_{dl}$ value for the Pt/Co-CCP catalyst.

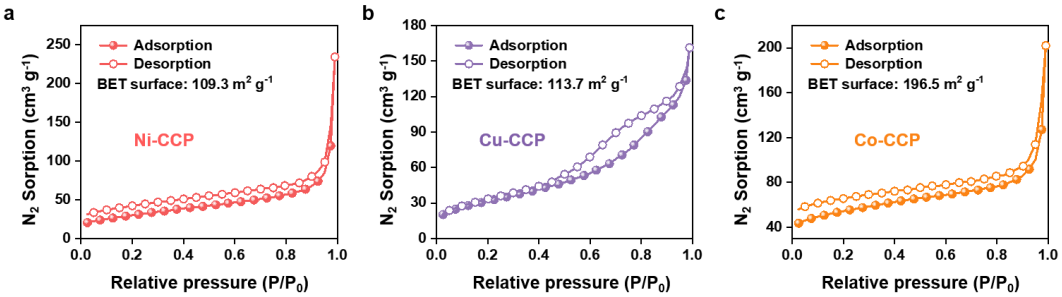


**Fig. S25.** $N_2$ desorption/adsorption isotherms for the Ni-CCP, Cu-CCP and Co-CCP from the BET measurements, respectively.

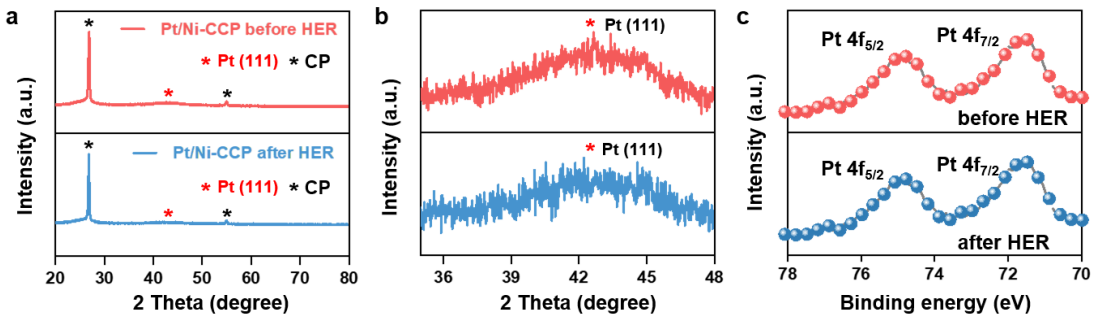


**Fig. S26.** (a, b) XRD patterns and (c) XPS spectra for the Pt/Ni-CCP before and after the acidic HER electrocatalysis, respectively.

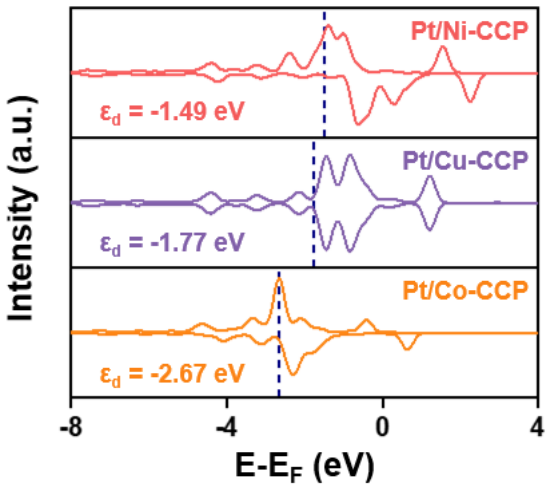


**Fig. S27.** Density of state analysis of Pt/Ni-CCP, Pt/Cu-CCP and Pt/Co-CCP. The *d*-band center ($\varepsilon_d$) values of the single-atom Ni, Cu and Co sites in Pt/Ni-CCP, Pt/Cu-CCP and Pt/Co-CCP are shown.

**Table S1.** Performance comparison between the Pt/Ni-CCP and other reported alkaline HER catalysts.

| Catalysts | $\eta^1$ (mV) | Support | Stability (h) | Ref. |
|---|---|---|---|---|
| Pt/Ni-CCP | 36.7 | Carbon paper | 100 | This work |
| PtNiCuCoPd HEA | 38 | Carbon cloth | ≈ 96 | 1 |
| Pt-$NiO_x$/C | 39.6 | Carbon paper | 25 | 2 |
| Pt-$NiCo_2O_4$ | 40 | Ni foam | 100 | 3 |
| PtNiCuMnMo HEA | 44 | Alloy ingots | 72 | 4 |
| $Ni_2P$/CoP-Pt | 44.5 | Ni foam | 80 | 5 |
| Pt NPs@CF | 49 | Carbon foam | / | 6 |
| $P_{16}$-PtFeCoCuMo | 52 | GCE | 8 | 7 |
| Pt@LDH | 58.7 | GCE | 24 | 8 |
| HEA@KB | 61.4 | Ni foam | 90 | 9 |
| WC/C-4.0% Pt | 73 | GCE | 24 | 10 |
| PtRu/CNT@$MO_2$−x | 75 | Carbon paper | 24 | 11 |
| Pt/$Co_3O_4$-VG | 82 | Carbon cloth | 40 | 12 |
| Pt-NiCo LDO | 92 | GCE | 100 | 13 |
| Pt/Nb-$Co(OH)_2$ | 112 | GCE | 33 | 14 |

[1] Overpotentials at 10 mA/cm$^2$, currents are normalized to the projected geometric area.

**Reference**

1 Z. Yu, Y. Zhang, S. Yang, X. Liu, T. Gu, Y. Qi, Y. Li, F. Miao, Z. Yan, *Int. J. Hydrogen Energy* 2025, **135,** 48-55.

2 X. Zheng, X. Zheng, M. Gao, Y. Liu, H. Pan, W. Sun, *Angew. Chem., Int. Ed.* 2025, **64,** e202422062.

3 W. Cheng, Z. Cui, S. Xu, S. Cheng, N. Gao, M. Yang, H. Li, *J. Power Sources* 2025, **641,** 236891.

4 T. Gu, F. Yu, Z. Yu, Y. Qi, Y. Li, F. Miao, Z. Yan, *J. Colloid Interface Sci.* 2025, **688,** 308-316.

5 Y. Tan, J. Feng, H. Dong, L. Liu, S. Zhao, F. Lai, T. Liu, Y. Bai, I. Parkin, G. He, *Adv. Funct. Mater.* 2023, **33,** 2209967.

6 Q. Li, Z. Deng, D. Tao, J. Pan, W. Xu, Z. Zhang, H. Zhong, Y. Gao, Q. Shang, Y. Ni, X. Li, Y. Chen, Q. Zhang, *Adv. Funct. Mater.* 2024, **34,** 2411283.

7 Z. Deng, S. Zhang, F. Li, Y. Zhu, C. Shan, Y. Zhao, *J. Power Sources* 2026, **673,** 239723.

8 J. Huo, Z. Ma, Y. Wang, Y. Cao, Y. Jiang, S. Li, Y. Chen, M. Hu, Q. Zhai, *Small* 2023, **19,** 2207044.

9 X. Liu, Z. Chen, H. Meng, J. Chen, L. Yang, M. Jin, X. Wang, Z. Chen, *Small* 2025, **21,** e07116.

10 L. Dong, X. Zeng, H. Chen, L. Zhao, W. Fang, X. Du, Z. Huang, X. He, W. Li, D. Wang, *Int. J. Hydrogen Energy* 2025, **105,** 1384-1392.

11 C. Zhou, K. Ma, Z. Zhuang, M. Ran, G. Shu, C. Wang, L. Song, L. Zheng, H. Yue, D. Wang, *J. Am. Chem. Soc.* 2024, **146,** 21453-21465.

12 J. Huang, B. Ren, P. Li, X. Ma, Q. Wang, *J. Power Sources* 2025, **640,** 236695.

13 Y. Tian, Y. Luo, T. Wu, X. Quan, W. Li, G. Wei, M. Bayati, Q. Wu, Y. Fu, M. Wen, *Adv. Funct. Mater.* 2024, **34,** 2405919.

14 Y. Tian, M. Wen, A. Huang, Q. Wu, Z. Wang, Q. Zhu, T. Zhou, Y. Fu, *Small* 2023, **19,** 2207569.